ELECTRICAL PROPERTIES OF STRUCTURAL COMPONENTS OF THE CRYSTALLINE LENS

R. T. MATHIAS, J. L. RAE, and R. S. EISENBERG, *Department of Physiology, College of Health Sciences, Rush University, Chicago, Illinois 60612, and the Department of Ophthalmology, University of Texas Medical Branch, Galveston, Texas 77550 U.S.A.*

ABSTRACT The electrical properties of the crystalline lens of the frog eye are measured with stochastic currents applied with a microelectrode near the center of the preparation and potential recorded just under the surface. The stochastic signals are decomposed by Fourier analysis into sinusoidal components, and the impedance is determined from the ratio of mean cross power to input power. The data are fit by an electrical model that includes two paths for current flow: one through the cytoplasm, gap junctions, and outer membrane; the other through inner membranes and the extracellular space between lens fibers. The electrical properties of the structures of the lens which appear as circuit components in the model are determined by the fit to the data. The resistivity of the extracellular space within the lens is comparable to the resistivity of Ringer. The outer membrane has a normal resistance of 5 kohm · cm^2 but large capacitance of 10 $\mu F/cm^2$, probably because it represents the properties of several layers of fibers. The inner membranes have properties reminiscent of artificial lipid bilayers: they have high membrane resistance, 2.2 megohm · cm^2, and low specific capacitance, 0.8 $\mu F/cm^2$. There is so much membrane within the lens, however, that the sum of the current flow across all the inner membranes is comparable to that across the outer surface.

INTRODUCTION

The electrical properties of the crystalline lens of the eye are of interest for several reasons. The properties are measures of the functions of the membranes and cytoplasm in health and disease, and alterations in some of the properties certainly accompany, and may even precede, the formation of cataracts. The electrical properties are also one measure of the transporting characteristics of the membranes of the preparation. From a more general point of view, the lens is an archetypical electrical syncytium, a tissue composed of many cells, electrically coupled one to another, with an extracellular space pervading the tissue. The electrical properties and relevant structure of the lens have been reviewed recently in some detail (Rae, 1978) and that paper should be consulted for further discussion of the role of the electrical properties in the normal function of the lens.

An important stage in the analysis of any tissue is the construction of a paradigm, a model which allows understanding of the main properties of the preparation. The gross properties of the lens are similar to those of a giant spherical cell (Duncan, 1969, 1973; Rae, 1973, 1974) and so the expected properties of a giant spherical cell might be a suitable paradigm (Eisenberg and Rae, 1976). The lens is composed, however, of many small fibers, coupled by gap junctions (Cohen, 1965; Benedetti et al., 1976), and containing an extensive extracellular space (Paterson, 1970), which should produce a pattern of current flow much more

complex than that in a simple spherical cell. An analogy exists with a similar situation in the study of skeletal muscle (Eisenberg et al., 1977). Skeletal muscle contains a pervading extracellular space in its "transverse" tubular system and yet can be approximately described by the fairly simple equations of one-dimensional cable theory modified to include the tubular system as an extra pathway by which current can leave the cell cytoplasm (Jack et al., 1975, Chap. 6). A similar but simpler situation may be expected in the lens. Because the sphericity of the preparation prevents longitudinal potential gradients, to some approximation all the lens interior is expected to be at the same potential. But gradients of potential across membranes within the lens are possible (even at this level of approximation) because current flow in the extracellular space can induce significant potential drops. If one qualitatively takes into account point source effects near the current microelectrode (Eisenberg and Johnson, 1970), it is possible from this analogy alone to draw an equivalent circuit of the lens, but such a circuit would not include the relation between the circuit elements and the real morphological entities which make up the preparation. For that reason, the equivalent circuit needs to be determined by a theoretical analysis (Eisenberg et al., 1979) of the current flow expected in a spherical syncytium. The differential equations solved by Eisenberg et al. (1979) and Peskoff (1978) can be derived from the flow of current in a small but finite volume element. Barcilon et al.[1] have shown how similar differential equations can be derived from more fundamental principles.

For this theory to serve as a paradigm for the lens, it is necessary to see how well it describes the behavior of the preparation as measured in a number of ways in a variety of conditions. This paper begins that process, and determines a number of properties of interest, by analyzing the linear electrical properties of the lens measured over a wide range of frequencies. Measurements are made in the frequency domain (that is, with random current signals analyzed as a sum of sinusoids) instead of in the time domain (that would be with step functions of current) because frequency domain analysis often is a much more sensitive measure of electrical properties (Eisenberg et al., 1977). Random signals are used because they permit much faster measurements than sinusoids; in our apparatus it is possible to acquire 800 independent data points from, for example, 0 to 80 Hz in steps of 0.1 Hz in the same time it would take to measure the response to a sinusoid of 0.1 Hz (namely, about 100 s).

Our results (Mathias et al., 1978) are determined by fitting the theoretical model of a spherical syncytium to the impedance measured from the lens over a wide range of frequencies. The excellent fit of the theory to the experimental data demonstrates the adequacy of the theory and determines the electrical properties of the surface and inner membranes of the preparation. Both the surface and inner membrane systems contribute importantly to the overall electrical properties: the surface membrane because of its typical conductance (despite its relatively small area); the inner membrane because of its enormous area (despite its small conductance). There is no a priori necessity that the curve fitting procedure should find both systems of membranes to be important; in fact the data presented here are sensitive measures of the paths for current flow and should be viewed as independent evidence for (*a*) electrical coupling between lens fibers, (*b*) current flow across inner membranes into an

[1]Barcilon, V., R. S. Eisenberg, and R. T. Mathias. Microscopic and macroscopic description of the electrical properties of syncytial tissues. Manuscript in preparation.

extracellular medium pervading the interior of the lens, (*c*) significant potential decrement in that extracellular medium, (*d*) unusually low conductance for the inner membranes, (*e*) comparable total conductance for the inner and surface membrane systems.

METHODS

All measurements reported here were made on small (1–2 in.) grass frogs, *Rana pipiens*. Animals of this size had lenses of about 0.16 cm radius which were nearly spherical (anterior-posterior/equatorial ratio $\simeq$ 0.8). Lenses of this small size have large enough input resistance to permit measurement of potentials induced by the microamperes of current which the current microelectrode would pass.

Because the resting potential of the lens is highly susceptible to trauma, no attempt was made to dissect the lens free of the globe. Rather, the globe was removed from the animal and its posterior portion was removed and discarded under direct microscopic observation. In addition, the cornea and iris were excised, leaving the lens suspended by its zonules from a ring of uveal-scleral tissue. With this procedure, virtually every lens dissected had an acceptable resting potential (more negative than −60 mV, mean −68 mV) and resistance. It is unlikely that this surrounding ring of tissue could have offered any appreciable resistance to current flow from the lens as a space separating the lens from the tissue could always clearly be seen.

After dissection, the lenses were carefully pinned into the experimental chamber by sticking 00 insect pins through the uveal-scleral ring into the transparent Sylgard (Dow Corning Corp., Midland, Mich.) layer which lined the bottom of the chamber. A light was then shone through the preparation from below to allow the determination of the degree of lens transparency. Lenses that were not clear were discarded. The bathing chamber was filled with a special Ringer's solution whose composition is slightly different from that used by other investigators utilizing amphibian tissue, namely (in mM/liter), $[Na^+]$ = 106.6, $[K^+]$ = 2.5, $[Ca^{++}]$ = 2, [Cl] = 114, $[H_2PO_4^-]$ = 0.35, and $[HPO_4^{--}]$ = 0.85, with pH 7.3. This solution had an osmolality of 210–215 mosmol/liter instead of the customary 240 mosmol/liter (Adrian, 1956) and was found to keep the lens resting potential stable for the duration of most experiments; in addition, it kept the lens in a crystalline, transparent state. Investigations in which lenses of the same size were viewed directly using Hoffman modulation contrast microscopy techniques, showed that the epithelial cells of the lens were shrunken when a solution of 240 mosmol/liter was used, whereas they were swollen if a solution $<$210 mosmol/liter was used, normal volume being that observed in a preparation not exposed to any Ringer solution. We are therefore confident that our bathing solution was appropriate.

The lens was penetrated by two microelectrodes, one for passing current and one for measuring the potential difference induced by the current flow across resistive and capacitive elements in the tissue. The current electrode was a glass capillary microelectrode filled with a mixture of 1.8 M K^+ citrate and 0.8 M KCl, pH ~7. This solution has been found to help the electrode pass depolarizing current (Valdiosera et al., 1974*a*). This property is important here because currents on the order of 500–1,000 nA were necessary to induce easily measurable voltages. The current electrode typically had a resistance of about 20 megohms. The voltage measuring electrodes were filled with 3 M KCl and typically had a resistance of 3–5 megohms. Only electrodes having tip potentials of $<$4 mV were used. The electrodes were placed in the lens under direct observation through a Hoffman modulation contrast microscope (McBain Instruments, Chatsworth, Calif.) at a magnification of about x100. In these studies, the current microelectrode was placed near the center of the lens as determined by simply viewing the penetration of the current electrode. The transparency of the lens made this approach possible, whereas such an approach probably would not be adequate for other tissues. The voltage measuring microelectrode was placed in the lens just under its surface. Its depth was estimated to be between 100 and 200 μm below the lens surface. The effect of positioning errors can be determined from Eq. 24, and neighbors, in Eisenberg et al. (1979). The only significant effect occurs in the variable $R_s(r, R, \theta)$ and, just for this reason, we do not attempt to derive physiological information from the value of R_s.

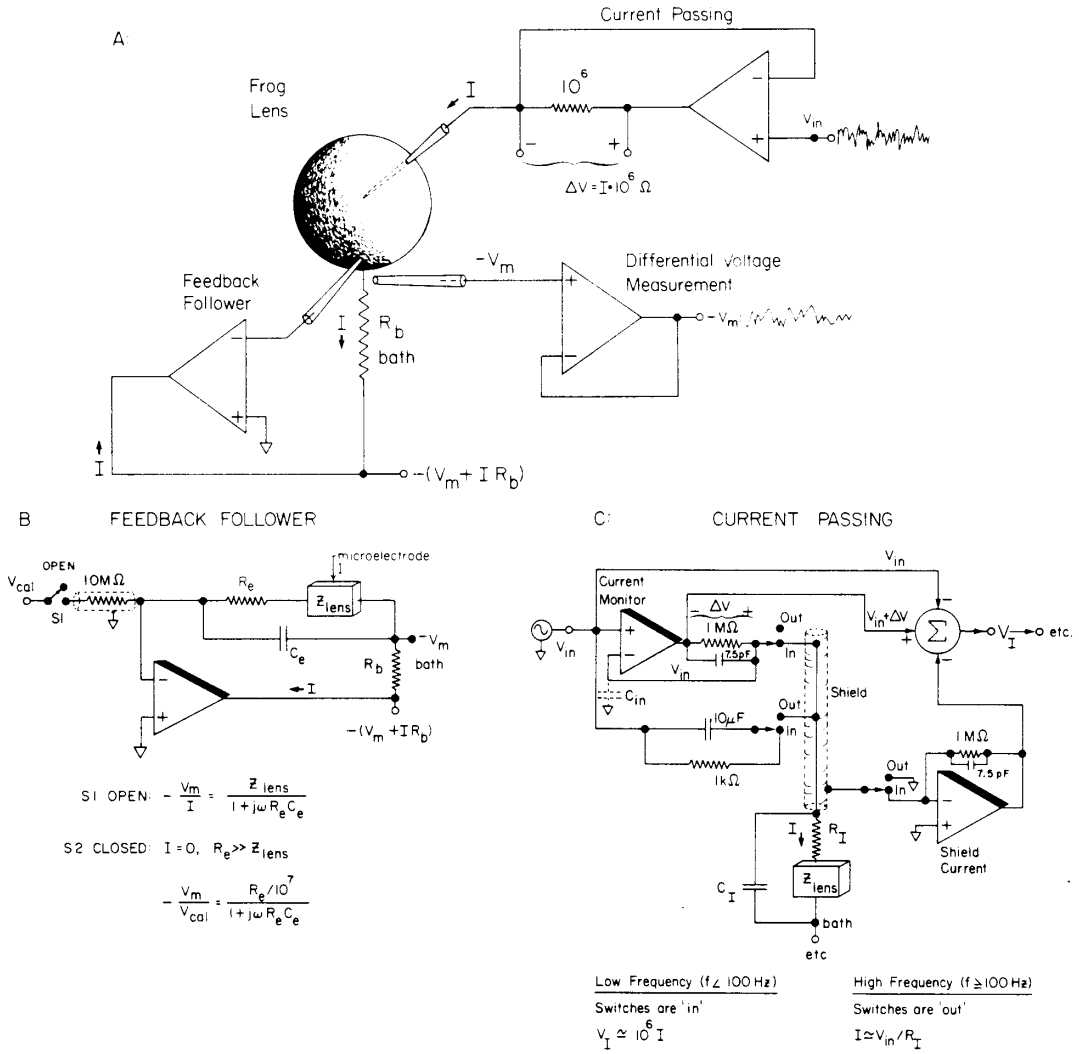

FIGURE 1 (A) A schematic description of the set-up. (B) A reasonably complete diagram of the feedback follower. The circuit applies current to the bath through the bath electrode of impedance R_b to hold the summing junction (and thus usually the tip of the microelectrode) at virtual ground. C_e is the capacitance from the microelectrode into the bath. Current is injected into the preparation with another microelectrode and the resulting potential is indicated for the normal case when switch S1 is open. The V_{cal} signal is used to measure the resistance and time constant of the microelectrode. Closing the switch S1 and setting $I = 0$ allows simple measurement of R_e, resistance of the microelectrode, and R_eC_e, the time constant of the microelectrode. (C) The current monitor circuit. When all the switches are in the IN position, the circuit estimates the current flowing through the tip of the current microelectrode into the preparation. The current monitor circuit itself (in the upper left-hand part of the figure) applies the voltage V_{IN} to the top of the current microelectrode and measures the applied current by the IR drop ΔV. The current leaving this circuit does not all cross the preparation, however, because some flows through the capacitance C_I into the bath, some flows into the shield of the cable, and some flows into the conductive paint applied to the current microelectrode. The latter two currents can be measured by the "shield current" circuit shown and subtracted from the signal ΔV to give an improved estimate of the current flows through the preparation. At frequencies above 100 Hz, significant current flows through the unshielded capacitance C_I. Thus, above 100 Hz the current monitor is removed from the circuit by placing the switches in the OUT position, and current is determined from the voltage applied and the resistance of the current microelectrode.

The circuit used for the electrical measurements is shown in Fig. 1. Minimizing the resistance from bath to the output of the feedback follower proved to be a matter of considerable importance. This was done by collecting the current from the bath through six Ringer-agar bridges connected in parallel. Each bridge extended from the bath into its own individual well, filled with 3 M KCl. The bath electrode was a silver-silver chloride pellet electrode in a microelectrode holder (W-P Instruments, Inc., New Haven, Conn.). With this arrangement, the resistance of the bath electrodes was about 750 ohm, the resistance being measured directly by passing current and measuring the potential induced in the bath.

The measurements were made by passing wide band noise currents through the current microelectrode, currents generated by applying the output of a white noise generator (Hewlett-Packard, Co. Palo Alto, Calif., model 3722A) to the V_{in} terminal shown in Fig. 1. The total current applied to the current microelectrode was continuously measured. However, not all of the current that is applied to the microelectrode goes through the preparation. Some of it goes through the walls of the microelectrode, enters the bath, is collected by the bath electrodes but never enters the preparation. We attempted to minimize this error in the following manner. First, we shielded the current electrode with silver paint to within 2 mm of the tip. This silver paint was covered with nonconductive varnish to isolate the shield from the bath. This continuous shield around the current electrode was connected to another current measuring circuit. The current collected in this circuit was subtracted from the total current going through the microelectrode, thus improving our estimate of the current going through the preparation itself. The presence of the capacitances C_I and C_{in} prevents the perfect estimation of the current going through the preparation. At frequencies above 100 Hz, significant current flows through them so the current monitor is removed from the circuit. Above those frequencies, current is determined from the voltage applied to the microelectrode and its previously measured resistance. The intracellular voltage electrode was also surrounded by a grounded shield although no silver paint was used. This shielding arrangement substantially reduced the capacitance between the microelectrodes.

The voltage measurement was made with a somewhat unusual circuit (Eisenberg and Gage, 1969). The intracellular voltage electrode, the preparation, the bath resistance, and the parallel current collecting electrodes were placed in the feedback loop connected to the inverting input of the measuring operational amplifier. This arrangement holds both the intracellular voltage electrode and the isopotential component of the lens potential at virtual ground. As a result, the stray capacitance between the voltage microelectrode and ground is reduced by the open loop gain of the operational amplifier, the frequency response being limited by the capacitance C_e into the bath. The bath is then held at minus the potential at the tip of the voltage microelectrode by the output current of the operational amplifier. Because the current flowing through the preparation also flows across the bath resistance and the resistance of the bath electrodes, the potential at the output of the feedback follower is then the sum of the intracellular potential, the IR drop in the bath, and the IR drop in the bath electrode. The IR drops can be eliminated by measuring the extracellular potential with another microelectrode located just outside the lens. The potential measured is then independent of IR drops in the bath or bath electrodes. With the current electrode in the center of the lens, it was verified that the location of the second voltage measuring electrode was not important, so long as it was close to the lens. In practice, we always placed the extracellular voltage electrode just outside the penetration site of the intracellular voltage microelectrode. The extracellular voltage electrode was partially covered by a driven shield to minimize the stray capacitance to ground. The output of the operational amplifier measuring the potential on the bath microelectrode, which in this case was the real intracellular potential, was fed into one channel of a Nicolet Fourier analyzer (model 401A, Nicolet Scientific Corp., Northvale, N.J.). The output V_I from the current measuring circuit was fed into the other channel. The Fourier analyzer passes each analog signal through a steep low pass filter which reduces aliasing errors (for white noise input) to at least 70 dB below the signal level. The signals are then sampled and digitized in a strictly linear 11 bit analog-to-digital converter and blocks of data (usually 1,024 points in duration) are processed by discrete Fourier transform with sufficient guard digits to preserve a dynamic range of 70 dB. The

Fourier transform of the input, the current signal, denoted by $X(j\omega)$, and the output, the voltage signal, denoted by $Y(j\omega)$, are then converted to estimates of the power spectrum of the input $G_{xx}(j\omega)$, of the output $G_{yy}(j\omega)$, and of the complex quantity, the cross power $G_{xy}(j\omega)$, by the formulas $G_{xx}(j\omega) = X(j\omega)X^*(j\omega)$; $G_{yy}(j\omega) = Y(j\omega)Y^*(j\omega)$; $G_{xy}(j\omega) = X^*(j\omega)Y(j\omega)$, where * denotes the complex conjugate of the immediately preceding complex variable. Again sufficient digits are processed to preserve a dynamic range of 70 dB in all results, including subsequent estimates of transfer function.

It is necessary to average repeated blocks of data from the same system both to reduce variance inherent in probabilistic estimates of the properties of the preparation (Oppenheim and Schafer, 1975, chap. 11) and to reduce variance introduced by extraneous noise generated in the voltage recording microelectrodes and apparatus (Bendat and Piersol, 1971, p. 142). Averages must be taken of the power spectra (not of $X(j\omega)$, $Y(j\omega)$, or of the transfer function itself) to remove these difficulties without introducing worse problems. Thus, the mean values $\overline{G}_{xx}(j\omega)$, $\overline{G}_{yy}(j\omega)$, and $\overline{G}_{xy}(j\omega)$ are used to compute estimates of the transfer function of the preparation $\overline{Z}(j\omega) = \overline{G}_{xy}(j\omega)/\overline{G}_{xx}(j\omega)$, and of the coherence function $\gamma^2(j\omega) = |\overline{G}_{xy}(j\omega)|^2/\overline{G}_{xx}(j\omega)\overline{G}_{yy}(j\omega)$. The solidi $|\ |$ denote the magnitude of the enclosed complex variable. The coherence function is a real number between zero and one. It equals unity at all frequencies in a linear noise-free system measured with a perfect Fourier analyzer (Bendat and Piersol, 1971). If the system is nonlinear, the coherence function is reduced, although the amount of the reduction is not simply related to traditional measures of nonlinearity such as harmonic distortion. If the system is linear, and the input to the system (here the current signal) is free of contaminating noise, the coherence function at each frequency is a measure of the output signal to noise ratio $S_n(j\omega)$ at that frequency, namely, $\gamma^2(j\omega) = S_n^2(j\omega)/[1 + S_n^2(j\omega)]$, where the signal to noise ratio is that of the voltage signal $Y(j\omega)$, measured in units of (volts-root mean square)/(volts-root mean square), not in units of a ratio of powers.

The transfer function measured by the Fourier analyzer is a probabilistic estimate of the impedance of the preparation at the discrete, evenly spaced frequencies appropriate to the discrete Fourier transform. Conversion of this estimate into one comparable to that determined with sinusoids requires further data processing, both to reduce variance and to produce a more appropriate spacing of frequency points.

Resolution, Bandwidth, and Merging

The electrical properties of the lens, and most electrical circuits for that matter, extend over a wide range of frequencies, showing rapid variation in the lower frequency range and slow variation in the higher frequency range. For this reason it is convenient and conventional to plot the properties of such a preparation with a logarithmic frequency scale, the log function providing the resolution at low frequency necessary to illustrate the rapidly varying properties and the compression at high frequencies necessary to illustrate the slowly varying properties. The data measured here, however, are spaced at constant intervals of frequency, with a constant resolution over the entire band of frequencies examined. This spacing is a fundamental property of the discrete Fourier transform used to compute the data. A discrete Fourier transform of a single block of data does not provide the resolution at low frequency or the compression at high frequencies needed to best illustrate the properties of the preparation. We must acquire several blocks of data from the same preparation to solve this problem.

The resolution at low frequency needed here is some 0.0125 Hz. Inasmuch as our digital system deals with 400 frequency points in one block ("data set"), this data set provides information from DC to 400 × 0.0125 Hz = 5 Hz. To cover the bandwidth of interest (here extending to 1 kHz), three other data sets are taken from the same preparation: one with a resolution of 0.05 Hz, extending to 20 Hz; another with a resolution of 0.25 Hz, extending to 100 Hz; and finally one with a resolution of 2.5 Hz, extending to 1 kHz.

The data from such a set of measurements are shown on a logarithmic scale in Fig. 2. Individual frequency points are shown to emphasize that each is an independent measurement and to illustrate the variance of the measurements. The data map out the electrical properties over the entire frequency

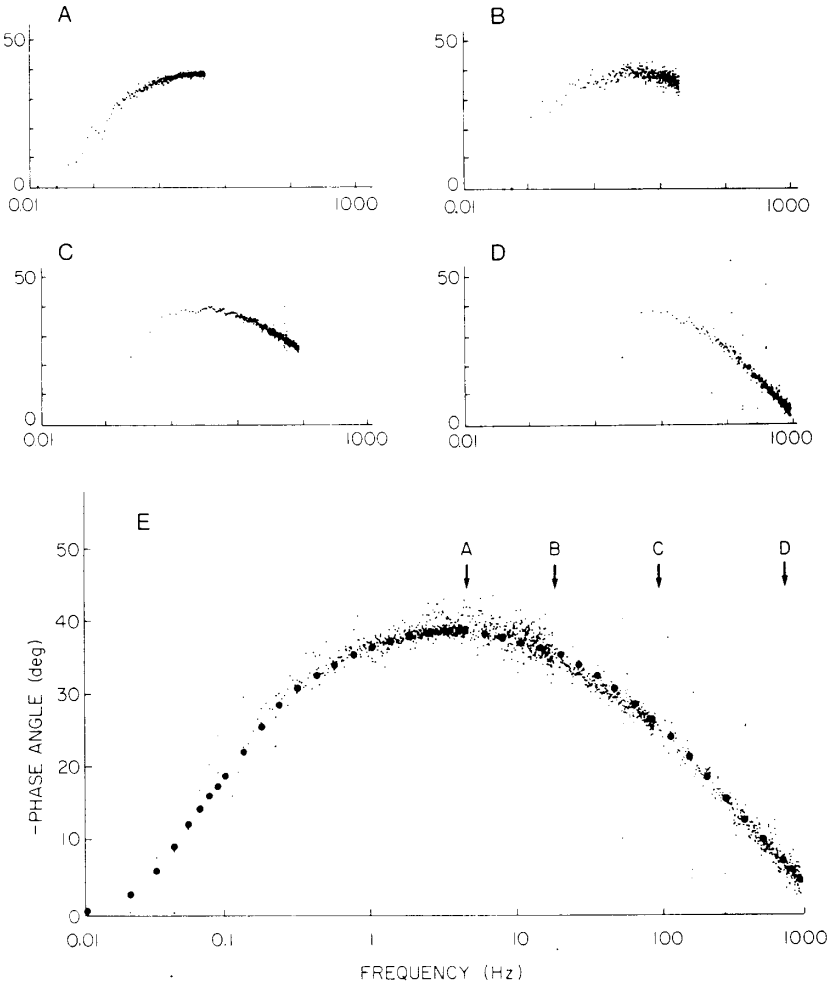

FIGURE 2 Raw measurements of the phase angle of the lens impedance. Each point represents an estimate of the phase angle at a given frequency determined by Fourier analysis and subsequent data processing (see text). Each small panel represents the mean of data blocks taken with a given resolution and bandwidth.

	Resolution (lowest frequency)	Bandwidth (highest frequency)	No. of data blocks averaged
	Hz	*Hz*	
A.	0.0125	5	16
B.	0.05	20	32
C.	0.25	100	32
D.	2.5	1,000	128

Panel E shows overplots of the data sets A D with arrows indicating the highest frequency point in each data set. The filled circles show the results of editing, smoothing, and merging.

The duration of one block of data is the reciprocal of the resolution. The number of frequency samples is the bandwidth divided by the resolution. The number of time samples needed to determine this number of frequency points is set by the Nyquist sampling requirements and the slope and maximum attenuation of the anti-aliasing low pass filters. In our apparatus the frequency of sampling is 2.56 times the bandwidth.

range of interest, with overlapping data in a number of regions. A composite data set must be made from these multiple data blocks to summarize compactly the properties of the preparation. This composite is made by a process which involves several steps: (*a*) each block of data is edited to remove "wild points," which would otherwise badly contaminate the subsequent data, (*b*) each block of data is smoothed to reduce variance (at the expense of resolution) and to produce data approximately evenly spaced on a logarithmic frequency scale, and (*c*) the data are merged to form the final data set used for subsequent analysis.

The wild point editing consists of a preliminary smoothing of the data, using a digital low pass filter, and computation of the standard deviation of the data set using the formula

$$(\mathrm{SD})^2 = \sum_{f_i} \frac{\{(\text{smoothed datum at frequency } f_i) - (\text{raw datum at } f_i)\}^2}{\text{Number of frequencies} - 1}.$$

Raw data that deviated too far from the preliminary smoothed value at that frequency, typically some 2 SD or more, were considered wild points and were replaced with the smoothed value at that frequency. The other data points were not changed and so the details of the preliminary smoothing are of no consequence. Most of the wild points occurred at multiples of the power line frequency.

Next, it is necessary to smooth the data by averaging neighboring data points, thus trading a reduction in the number of independent data points for a reduction in variance. The reduction in the amount of data is just as important in our application as the reduction in variance, because the curve fitting procedure used later to confront theory with experiment cannot easily deal with more than some 80 data points. The smoothing procedure used here is "triangular weighting" because it is easily modified to include a variable number of neighboring points. Each datum $\bar{z}(f_i)$ at frequency f_i was replaced by the weighted average $z(f_i)$ of the data at the neighboring frequencies f_j, ranging from the lowest frequency f_{i-n} through the highest frequency f_{i+n}. The weights were chosen to decrease linearly as the frequency f_j moved further from the center frequency f_i, hence the name "triangular weighting." The procedure is precisely specified by

$$\bar{z}(f_i) = \sum_{j=n}^{0} w(j)\, z(f_{i-j}) + \sum_{j=1}^{n} w(j)\, z(f_{i+j})$$

where the weights $w(j)$ are $w(j) = [1/(n+1)](1 - j/(n+1))$ for $j = 0, 1, 2 \ldots, n$. The coefficient $1/(n+1)$ is chosen so that $\bar{z}(f_i) = z(f_i)$ if the data at all frequencies are the same.

As pointed out previously, it is desirable to select points from each block of data that are separated by approximately constant intervals of log frequency. The points selected at the high end of the frequency range will be, of course, much further spaced than those at the low end. Thus, it is important that the points chosen at high frequency should reflect the value of many more neighboring points than those chosen at the low frequency end. In other words, n should vary with frequency.

More precisely, to achieve a constant logarithmic weighting one wishes $\log(i+n) - \log(i-n)$ to be a constant, which implies that $n = \alpha i$. (The equal sign should be read as "the integer part. . . .") The above procedure was used with $\alpha = 0.4$, provided $n < 50$. The number of averaged points was not increased beyond 101 (i.e. $n = 50$) because further reduction in variance seemed pointless (see Fig. 4). The very highest frequency points in each block (those within n spacings of the maximum frequency) require a special procedure. In that case we progressively reduced n from 50 to 24 until the datum $z(f_i)$ was 24 from the end of the data set. The last 24 data points were replaced by a linear extrapolation of the previous 24 and, whenever possible, were not subsequently used. We usually filled in the "hole" in the data by subsequent merging with another data set taken over a wider bandwidth.

The result of this entire procedure is to produce sets of smoothed data spaced almost uniformly on a logarithmic frequency axis. These smoothed data sets were then combined to form a merged data

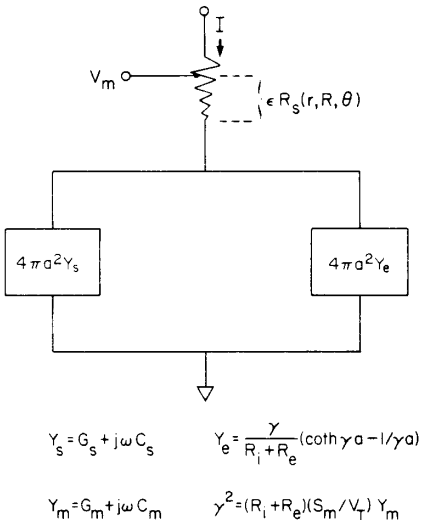

FIGURE 3 The distributed equivalent circuit of the lens. The circuit shown is a close approximation to the theoretical results of Eisenberg et al. (1979). The tapered resistor at the top of the figure represents the resistance to the flow of current away from the current microelectrode, the point source effect. The voltage electrode measures a fraction of this point source effect, which fraction depends on the radial location of the current and voltage microelectrodes (R and r, respectively) and their angular separation θ. If the electrodes are close together just under the surface membrane $\epsilon R_s \rightarrow R_i/2\pi a\theta$. If one electrode is close to the center of the preparation and the other just under the membrane, $\epsilon R_s \rightarrow (R_i/4\pi a) \cdot ([a - r]/a + 3[\cos\theta][R/a])$. The other symbols are defined in the figure, Y_s being the admittance of the surface membrane and Y_e the admittance of the inner membranes. The propagation constant γ at DC is the reciprocal of the length constant.

set, examples of which are shown in Results. The procedure for merging was simply to switch from one data set to another near the high-frequency end of the lower-frequency data set. Smoothing was never done across data sets; that is, every smoothed point is computed from data in one block, taken in one time interval. Thus, drift in the properties of the preparation is immediately apparent as discontinuities in the final merged data set. Such discontinuities were usually negligible; if not, the data were rejected.

This fairly complex procedure produces data comparable to that measured using sinusoids at constant intervals of log frequency.

Theory

The circuit model used here to describe the electrical properties of the lens of the eye is shown in Fig. 3, which, together with Table I, includes most of the relevant equations, definitions, and explanations. The circuit model well approximates the solution to the partial differential equations derived by Eisenberg et al. (1979), Peskoff (1978*a*), and rederived by Barcilon et al.[1] from more fundamental principles. Those papers offer more detailed physical, mathematical, and physiological explanations of the origin and meaning of the circuit.

The current voltage relation of the circuit in Fig. 3 is $V(r, R, \theta; j\omega)/I_0 = 1/[4\pi a^2(Y_s(j\omega) + Y_e(j\omega))] + \epsilon R_s(r, R, \theta)$, where $\epsilon R_s(r, R, \theta)$ (ohms) is defined in Eq. 20 of Eisenberg et al. (1979); I_0 (A) is the applied current; r, R (cm) are the radial locations of the voltage and current microelectrodes, and their angular separation is θ(deg or rad); ω is the angular frequency in radians per second and equals 2π times the frequency in hertz; $j = (-1)^{1/2}$; and the other symbols are defined in the figure and Table I.

Fig. 7 shows a lumped approximation to the circuit actually used to describe the lens. This approximation is accurate when the length constant (crudely speaking, $1/\gamma$) is large compared to the radius a. The approximate circuit is an aid to understanding the qualitative properties of the lens and the properties estimated by step function measurements (e.g. Eisenberg and Rae, 1976). The numerical values attached to the circuit elements are computed by the formulas shown from the parameters reported in Table I.

RESULTS

The data presented were generated by measuring the intracellular potential produced by the current applied from an intracellular microelectrode placed near the center of the lens. This placement of the current electrode is important because only in this case is there spherical symmetry in the potential just outside the preparation. Measurements made with the current microelectrode just under the surface of the preparation showed a bath potential that varied sufficiently with position to distort the impedance data. Inasmuch as a theoretical analysis of asymmetrical bath potentials is not available, and would probably be difficult to use if it were, it seemed best to place the current electrode near the center of the preparation. The insignificance of asymmetries in the bath potential was checked in each experiment by making our differential measurements of potential (see Fig. 1) with two different locations of the extracellular microelectrode: one measurement with the extracellular microelectrode just outside the lens, close to the voltage recording electrode; the other measurement with the electrode just outside the lens, close to the point where the current electrode entered the preparation.

The insertion of the current microelectrode into the center of the lens produced little visible damage (which is easily noticed in the preparation because of its transparency) and not much change in resting potential. Only occasionally did the resting potential change more than 2 mV when the current electrode was advanced into the center of the preparation. Even in those cases, the resting potential usually returned to its original value in some 5–10 min. Lenses in which there was visible damage or a prolonged decline in resting potential were discarded.

The data collected is presented as plots of the impedance of the lens as a function of frequency. Although the current applied was a random wave form and contained a wide range of frequencies, the method of data analysis decomposes the random currents and voltages into their sinusoidal components. Each component has on the average the same properties as a measurement made of the voltage induced by a pure sinusoid of that frequency. Thus, the impedance measured at say 100 Hz with our technique is the same impedance that would have been measured with a 100-Hz sinusoid using more conventional techniques. Plots are presented of both the magnitude and phase angle of the impedance, the latter being most useful in determining the circuit parameters of the preparation.

Figs. 4 and 5 show the impedance measured from typical preparations and the fit of the theoretical functions (and thus the equivalent circuit shown in Fig. 3) to that data. The plots of the magnitude have a plateau at low frequency and decline monotonically with frequency, reaching a limiting value. The low frequency value is simply the DC resistance of the preparation; the monotonic decline in magnitude occurs as the membrane current becomes primarily capacitive and as the magnitude of the transmembrane potential declines. The phase plots show a concomitant behavior, having zero phase angle at sufficiently low fre-

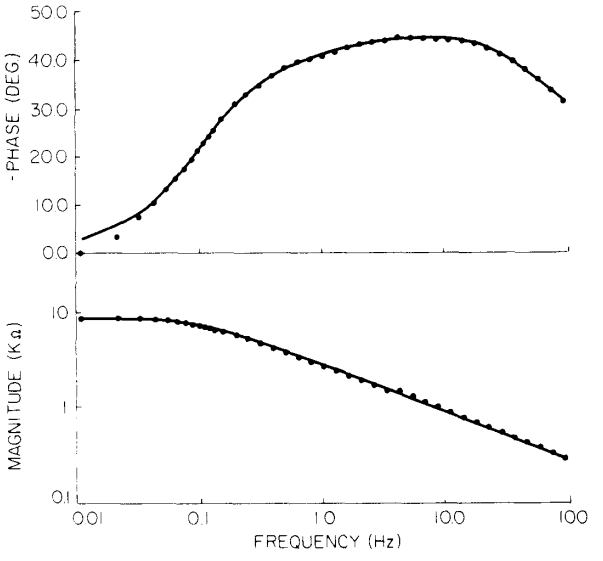

FIGURE 4 Plots of the magnitude and phase of the impedance of the lens. These plots were determined by application of current near the center of the lens and subsequent analysis of the induced potential as described in the text. The solid line is the theoretical curve determined by the best fit of the theory illustrated in Fig. 3.

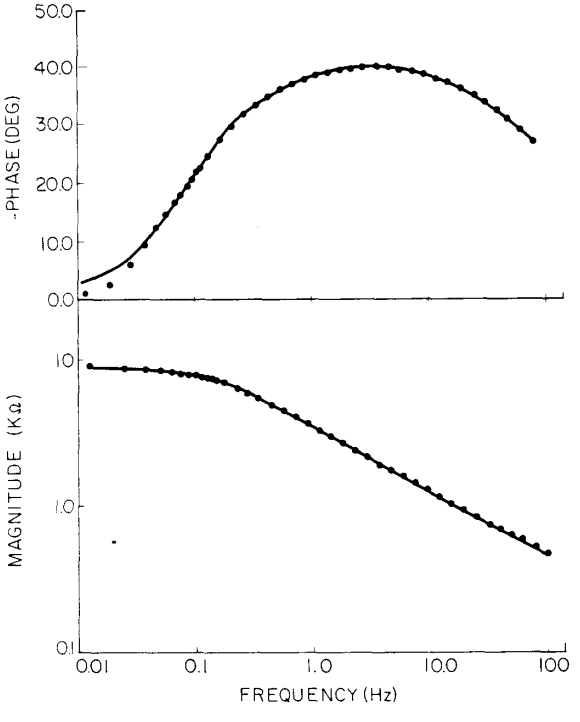

FIGURE 5 Plots of the magnitude and phase of the impedance of the lens.

quencies (where the impedance is essentially resistive), reaching a broad maximum, and then declining toward zero at sufficiently high frequency. Because the preparation behaves as if it has a resistance in series with all its membranes, at "infinite" frequency all the potential drop across the preparation occurs across this resistance and thus is in phase with the current.

Circuit parameters were determined by fitting the theoretical curves to the experimental data in the frequency ranges 0.1–100 Hz or, if available, to data in the frequency range of 0.01–100 Hz. The curve fitting techniques are described in Valdiosera et al. (1974*b*). One area of concern with curve fitting using multiple adjustable parameters is the uniqueness of the results. We have dealt with this problem in several ways. First, the curve shapes produced by a wide range of parameter values and combinations of values were determined to check whether the same curve could be produced in more than one way. Second, many different initial guesses of parameter values were used in the curve fitting process to show that the results were quite independent of the initial guess. Third, the curve fitting procedure was run with various parameters constrained to different values. This procedure determines whether the shape of the best fit theory curve is significantly altered if parameter values are set to other than their optimal value. Fourth, statistical measures of parameter reliability were calculated. The results of this analysis were clear: our parameter values are well determined by the experimental data except in one case, which involved both the internal resistivity R_i and the surface capacitance C_s. The effects of these parameters on the shape of the impedance curves is essentially reciprocal: the effects of an increase in R_i can be closely mimicked by a decrease in C_s. In other words, the high frequency time constant R_iC_s is well determined by the experimental data, but the individual parameters R_i and C_s are not. For this reason the value of $R_i = 625$ ohm · cm, determined by other methods (Eisenberg and Rae, 1976), has been adopted here. The other circuit parameters were well determined by the curve fitting procedure. For example, the standard deviation of the circuit parameters (a measure of the reciprocal of the derivative of the theoretical curve with respect to the parameters (see Valdiosera et al., 1974*b*, Eq. 12) is typically about 1% of the value of the parameters, being <2% even for C_s, providing R_i is fixed.

Multiple data sets have been taken from the same preparation in order to cover the entire frequency range of interest while preserving sufficient resolution at the low frequency end. It is possible to combine these data sets in a variety of ways and use each combination to determine circuit parameters. The variation of the circuit parameters from combination to combination is then a measure of at least two effects: one, the probabilistic nature of the data, which guarantees that two experiments will not give precisely the same result, and two, changes in the properties of the preparation or microelectrodes during the course of the experiment. We have fit all the possible combinations of data sets which span the frequency range DC–100 Hz and have computed the data shown in Table I by averaging the circuit parameters determined by curve fitting to each possible data set. The variation in the circuit parameters from data set to data set (of the same preparation) can be described by a standard deviation, which ranges from 3% of the mean for G_s to 12% of the mean for C_s. We see then that the merging process does not introduce a serious variance into our results.

Most of the data were taken in the frequency range 0.01–100 Hz because of the likelihood of systematic errors in theory and/or experiments at both higher and lower frequencies. The

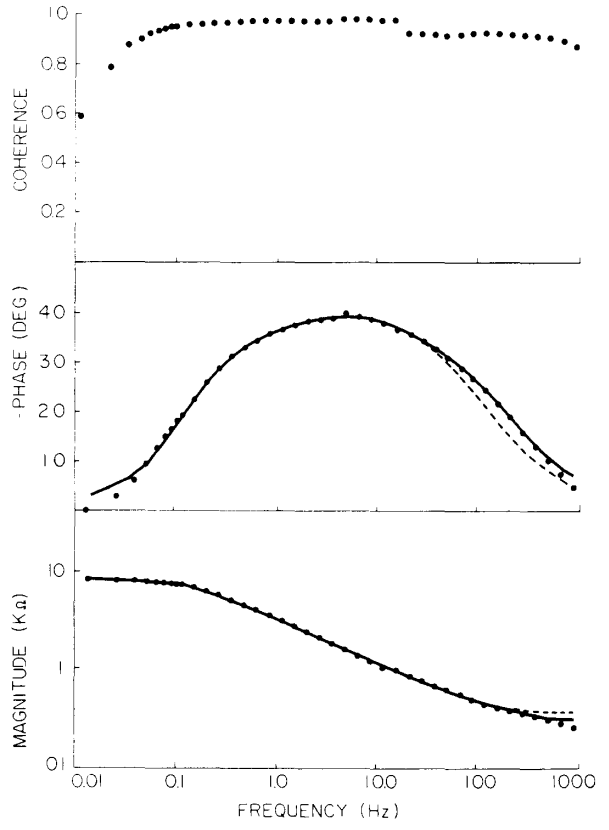

FIGURE 6 Plots of several fits of the theory to the magnitude and phase of the impedance of the lens. Here data is illustrated through 1 kHz. The theoretical curves indicate the best fit to data extending to 30 Hz (dashed line), 100 Hz, and 1 kHz (indistinguishable solid lines). The parameter values for each case are

	G_s	G_m	C_s	C_m	R_e	R_{test}
	mho/cm^2	mho/cm^2	$\mu F/cm^2$	$\mu F/cm^2$	$kohm/cm$	%
30 Hz	2.7×10^{-4}	3.8×10^{-7}	12	0.85	47	1.49
100 Hz	2.4×10^{-4}	4.9×10^{-7}	8.8	0.92	49	1.54
1 kHz	2.5×10^{-4}	4.4×10^{-7}	9.2	0.90	47	1.91

The coherence function illustrated has been determined from the original raw function by the same editing of wild points, averaging of neighboring points, and combining of different data sets described in the text. Thus, each point represents the average value of the coherence determined from exactly the same data that determined the final impedance point at that frequency. The discontinuity in the coherence function at some 20 Hz is not an error, but rather the consequence of a change in the amount of current applied to the preparation and thus in the signal-to-noise ratio of the recorded voltage.

systematic misfit at low frequencies evident in our data could have several explanations: the signal to noise ratio at these frequencies is very low (as was determined by examination of the coherence function, which gives a measure of signal to noise ratio), and this might introduce bias into the results as well as severe variance. It is also possible that there is some process not modeled by the theory which is most evident under these conditions. The good-

ness of fit at high frequencies is rather surprising and led us to extend the frequency range to 1 kHz in some of the later experiments. Results over the extended frequency range are shown in Fig. 6. Several theoretical curves are also shown in the figure, each curve being computed from a different subset of the data. One curve was computed only from the data extending to 30 Hz, another curve from the data extending to 100 Hz, and finally one curve was computed using the data extending to 1 kHz. The fits and parameter values producing each fit are quite similar, within about 10%, which is near the limits imposed by the probabilistic nature of the data. This result shows that the parameters are quite well determined by the data at lower frequencies and are not very sensitive to the data at high frequencies. The fit of the theoretical curves even at 1 kHz is somewhat surprising because one might expect the theory to fail at such high frequencies, where the spatial decrement of potential is very steep, even in distances comparable to the width of a few lens fibers. Evidently, the shape of the phase plot is not terribly sensitive to these effects.

A summary of our results is shown in Table I, which also includes estimates of the morphometric parameters and some of the relevant derived quantities (see also Fig. 7). Because the major source of variance in the results is the variation from preparation to preparation (probably biological in origin), the standard deviations are computed directly from the mean parameter values of each preparation. The parameter $\epsilon R_s(r, R, \theta)$ is the series resistance, which depends on the radial location of the voltage electrode r, the radial location of the current electrode R, and the angular separation between electrodes θ (see Eq. 20 of Eisenberg et al., 1979). However, potential drops not included in the theoretical model, due to certain artifacts which might be introduced by the experimental apparatus and procedure, also could be described by a series resistance. We have little reason to suspect serious difficulties

TABLE I
PARAMETERS OF LENS

Parameter	Mean value	SD,* $n = 10$	Source
		%	
G_s, surface membrane conductance	2.1×10^{-4} mho/cm^2	29	Curve fit
G_m, inner membrane conductance	4.4×10^{-7} mho/cm^2	34	Curve fit
C_s, surface membrane capacitance	9.8×10^{-6} F/cm^2	40	Curve fit
C_m, inner membrane capacitance	0.79×10^{-6} F/cm^2	20	Curve fit
R_e, effective extracellular resistivity	48×10^3 ohm-cm	21	Curve fit
a, radius	0.16 cm	4	Measured
R_i, effective intracellular resistivity	625 ohm-cm	—	Eisenberg and Rae, 1976
S_m/V_T surface of inner membrane per unit volume	6000 cm^{-1}	—	Rae and B. Eisenberg‡
$\epsilon R_s(r, R, \theta)$, series resistance	230 ohm	23	Curve fit
R_{test}, goodness of fit	1.2%	42%	Curve fit
R_{input}, input resistance	9×10^3 ohm	—	Derived
$\epsilon \equiv R_i/(R_i + R_e)$	0.01	—	Derived
λ(d.c.), length constant	0.088 cm	—	Derived
λ(100 Hz), length constant	0.0026 cm	—	Derived
λ(1,000 Hz), length constant	0.0012 cm	—	Derived
Resting potential	68 mV	6	Measured

*Written as percent of mean value.
‡Personal communication.

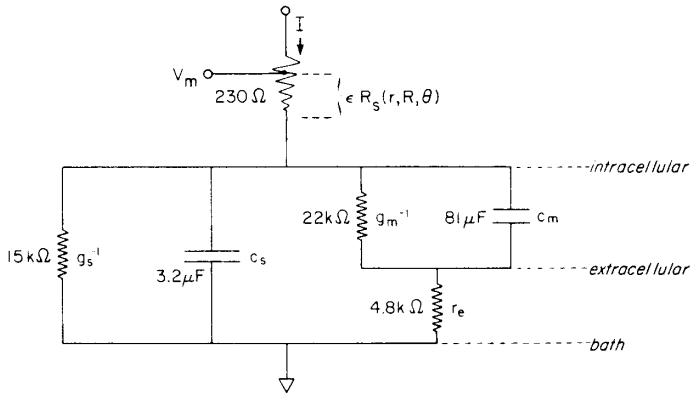

FIGURE 7 A lumped approximation to the equivalent circuit. This approximation is valid when $1/\gamma$ (crudely speaking, the length constant) is large compared to the radius a of the lens; it is useful both as a guide to qualitative reasoning and as a description of properties at low frequencies. The parameter R_s measures point source effects and is described in more detail in the caption to Fig. 3 and in Eisenberg et al. (1979). The other parameters are defined by $g_s = 4\pi a^2 G_s$, $c_s = 4\pi a^2 C_s$, $g_m = (4/3) \cdot \pi a^3 (S_m/V_T) G_m$, $c_m = (4/3)\pi a^3 (S_m/V_T) C_m$, $r_e = (R_i + R_e)/(20\pi a)$. The numbers shown are computed from the experimental results shown in Table I and indicate the significance of the two pathways for current flow, surface and interior, and of the resistance within the extracellular space.

in the theoretical model or experimental techniques, but we did not measure the electrode location with sufficient accuracy to convert ϵR_s into an estimate of the internal resistivity R_i. The parameter ϵR_s is not further used in the paper; it serves as a buffer to insulate our conclusions from the effects of local potential and various possible errors in theory and experiment. The parameter R_{test} is a root mean square measure of the deviation between theory and experiment (Valdiosera et al., 1974*b*). R_{input} is the ratio of steady potential to a steady applied current, with the electrodes far separated. The parameter ϵ is defined in Table I and plays a key role in the theoretical analysis (Eisenberg et al., 1979). The length constant λ is defined as the reciprocal of the real part of γ, which is itself defined in Fig. 3 and in Eisenberg et al. (1979). The length constant is a measure of the distance in which the extracellular potential changes by a factor of approximately e, and therefore is a measure of the spatial uniformity of the *trans*membrane potential across the membranes within the lens.

DISCUSSION

Qualitative Analysis and Significance of Results

Although the analysis presented in this paper is somewhat complex, the main conclusions concerning the properties of the surface and inner membranes can be predicted from an intuitive analysis of the magnitude plot in Figs. 4 and 5 and the lumped approximate circuit in Fig. 7. The magnitude plot has a corner frequency around 0.2 Hz, indicating that the first (slowest) time constant of the preparation is around 1 s. Because the input resistance of the preparation is about 10 kohm, the input capacitance must be on the order of 100 μF to produce the time constant of about 1 s. Biological membranes invaiably have a specific capacitance near 1 μF/cm^2, which implies that current applied to the lens must be charging at least 100 cm^2 of membrane to produce the measured time constant. The outer surface area

of the lenses used here is <0.5 cm^2, so the inner membranes must also be charged by the current applied with a microelectrode—there is no other way to provide the 100 cm^2 of membrane needed to account for the time constant of the preparation. The inner membranes are, in other words, in parallel electrical connection to the surface membrane and to one another. A parallel connection in turn implies that the extracellular and intracellular media allow substantial current flow; the extracellular medium is pervading but not isolated: it allows current to flow to the bath. The intracellular medium extends from the cytoplasm of one lens fiber to that of another, through gap junctions, and it also allows current to reach the outer membrane of the preparation and then the bath.

The above arguments can be extended to determine qualitatively the distribution of DC conductance between the surface and inner membranes. Because the inner membranes are charging their capacitances in parallel, and a membrane is represented electrically as a resistor in parallel with a capacitor, it follows that the conductance of these membranes must also appear in parallel, at least at DC. If the inner membranes had a typical conductance (that is, 0.1–0.4 mmho/cm^2), then the input resistance of the lens would be <100 ohm. Because the input resistance is about 10,000 ohm, we are led to the conclusion that the specific conductance of the inner membranes must be abnormally small.[2] Essentially all the inner membranes (even those in the nucleus of the lens) must have quite small specific conductance, because the presence of a substantial conductance in a parallel connection would produce a much lower value of input resistance than that observed.

Our results also show in both a qualitative and quantitative manner that all lens fibers are electrically well connected to one another. The steady voltage response to applied current is found to be quite independent of electrode location (see also Eisenberg and Rae, 1976), provided point source effects are avoided. That is, in the steady state all intracellular locations are at the same potential, and show the same input resistance; thus, all intracellular locations are electrically connected, presumably by the cytoplasm and numerous gap junctions between fibers.

Further Investigation

Further investigation is needed of our estimate of the effective extracellular resistivity, namely, 48 kohm·cm, because the effective resistivity depends on the volume fraction, the tortuosity, and the true resistivity of the solution filling the extracellular space, none of which has been independently measured. If one computes the tortuosity as suggested in the Appendix and estimates the volume fraction as 1.2% (Yorio and Bentley, 1976), the resistivity of the extracellular medium is 83 ohm·cm (Eq. A-1). The similarity of this figure to the resistivity of frog Ringer (some 91 ohm·cm) should not hide the number of assumptions made in its calculation.

Inasmuch as both the resistivity of the extracellular and intracellular media as reported here are "effective" parameters, further work is necessary to determine the actual resistivity

[2]It is theoretically conceivable that the effective resistance of the extracellular medium might be sufficiently high to limit the contribution of the inner membranes. Such is unlikely to be the case given the dimensions of the space. Both our quantitative results and an extension of the qualitative discussion of charging of the inner membrane capacitance show that the inner membranes contribute to the electrical properties measured.

of the two media. Morphological measurements of the orientation and density of gap junctions and extracellular space are a prerequisite for further theoretical and electrical analysis. Measurements of the spatial variation of impedance, perhaps using specialized electronics to remove the spatially uniform component of potential, would be useful in accurately determining the effective resistivities. Such measurements—both morphological and electrical—should be quite revealing of the anisotropic properties of the lens.

The value of the surface capacitance of some 10 μF/cm^2 also needs further investigation. It is much too large to represent the capacitance of a single unfolded sheet of membrane. The figure may possibly be in error, because it is such a small fraction of the total capacitance and because it might be sensitive to assumptions concerning, for example, the frequency independence of R_s. It is also possible that the figure is more or less correct but represents the composite properties of a number of membranes, probably the membranes of the outermost layers of fibers. Indeed, it seems likely that the boundary condition which Eisenberg et al. (1979) and Peskoff (1978) used to describe the outermost membrane of a spherical syncytium really describes the properties of the outermost layer of the syncytium. In that case the parameters ascribed here to the surface membrane certainly would represent the properties of a layer of fibers. There may also be a continuous gradation of membrane properties within the lens: then our theory and the resulting parameter values must be viewed as "mean values" of the true situation.

Physiological Role of the Inner Membranes

A significant finding of this investigation is that the inner membranes of the lens contribute importantly to the electrical properties of the tissue, but have insulating properties more reminiscent of lipid bilayers than of biological membranes (Fig. 7, Table I). The inner membranes are excellent insulators allowing only a few ions (per unit area) to cross from cytoplasm to extracellular medium. The total area of inner membranes is so large, however, that the total ionic current flow (across all the inner membranes) is about equal to the ionic current which flows across the surface membrane. Indeed, if the inner membranes did *not* have such unusual insulating properties, almost all the conductance of the preparation would be in its interior, in the combination of inner membranes and tortuous extracellular space. The insulating properties of the inner membranes serve to greatly reduce the amount of sodium pumping and therefore metabolism needed to maintain the viability of the tissue. Most biological membranes permit substantial leakage of sodium ions and water into their cytoplasm and so most cells must expend substantial amounts of metabolic energy to maintain ionic and osmotic gradients (Tosteson and Hoffman, 1960; Tosteson, 1964). If the inner membranes were not exceptionally good insulators, the lens would need a high density of sodium pump activity, accompanying metabolism, and subcellular organelles to maintain its ionic and osmotic gradients. But even then, there would be serious diffusional difficulties introduced by the tortuous extracellular space, and there might be optical difficulties as well, introduced by the subcellular organelles. Diffusion within the extracellular space could limit transport across the inner membranes, because the extracellular space within the lens is not a low resistance pathway (Fig. 7). Even though the resistivity of the solution within the extracellular space is close to that of Ringer's solution, the lumped resistance of the extracellular space is very high—comparable to the membrane resistance—

because of the small volume fraction and tortuosity of the extracellular pathways. Thus, ions transported across inner membranes would probably accumulate (or deplete) in "unstirred layers" within the extracellular medium.

It is thus difficult for the lens to accommodate a high volume density of sodium pump activity. It would also be difficult for the tissue to accommodate a large metabolic apparatus and still remain transparent. The large number of mitochondria needed to perform aerobic metabolism would certainly scatter light. A transparent tissue is also unlikely to include blood vessels, so all metabolism, anerobic and even aerobic if it were present, would be severely limited by long intracellular diffusion paths from the blood supply to the site of metabolism. For these reasons we expect the lens to have little ability to synthesize ATP.

The insulating properties of the inner membranes are thus seen as necessary if a transparent tissue is to contain inner membranes at all. The question remains, however, why does the lens contain inner membranes? It might be thought that they are a necessary consequence of the embryological development of the lens from many separate cells, but other giant cells, for example skeletal muscle fibers, are formed from the fusion of many small cells, whose plasma membranes then disappear (Fischman, 1972; Crowe and Baskin, 1977). It seems more likely that the inner membranes of the lens have either a mechanical function or a function related to the optical behavior of the tissue. Perhaps the inner membranes modify the index of refraction or transparency of the lens; perhaps they provide structural strength or other mechanical characteristics needed in a lens which focuses by deformation.

The speculative nature of the above discussion is justified, we hope, by its utility in suggesting experiments.

APPENDIX: THE TORTUOSITY FACTOR

The effective extracellular resistivity R_e reported in this paper is related to the actual resistivity of the extracellular solution $\bar{R}_e$ by the expression (Mathias et al., 1977)

$$R_e = \frac{\bar{R}_e}{\tau(V_e/V_T)}, \tag{A-1}$$

where the tortuosity factor τ is a measure of the effects of branching and convolutions of the extracellular space and V_e/V_T is the volume fraction of the extracellular space.

An analytical expression for the tortuosity factor has been derived as part of a theoretical analysis of random two-dimensional branching networks (Mathias et al., 1977; Eisenberg et al., 1977). The analysis has been shown numerically (Mathias, 1975) to be quite precise. The essential step in the analysis is the description of the two-dimensional branching in terms of only one spatial variable and a set of morphometric parameters. The difficulty in performing this step is that regular two-dimensional networks do not pack into the circular shape conventionally used to describe the boundary of the network. Thus, a geometric construction and probabilistic analysis is necessary to relate the measured properties of the two-dimensional network to the electrically important tortuosity factor.

It is likely that a similar analysis could be performed for the three-dimensional network of extracellular clefts, if those clefts had sufficient symmetry. Indeed, the recent theoretical results of Barcilon et al.[1] provide a guide to such an analysis and a linkage of that analysis to the theory used here. Such an analysis, however, requires morphological information not presently known. For example, an analytical description of the three-dimensional structure of the lens fibers and the anisotropic morphometric parameters of the extracellular space are not known. We can, however, proceed rather far by exploiting the quasi-crystalline nature of the lens and an oversimplified view of

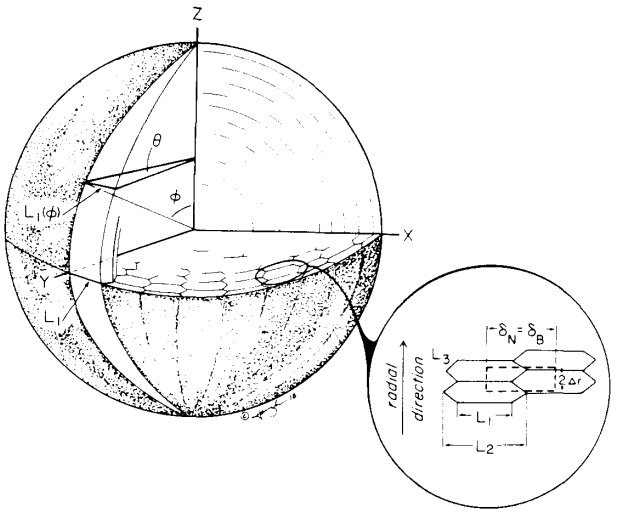

FIGURE 8 A representation of the structure of the lens. The angle θ defines a lune which represents one side of a hexagonal lens fiber. The length of that side is called $L_1(\phi)$, in general, to indicate its dependence on location, and is called L_1 at its maximum, when $\phi = \pi/2$.

the packing of lens fibers in which fibers run from north pole to south pole (Fig. 8). Instead of writing the tortuosity factor as a function of measured morphometric parameters (the only viable approach in a random network), we will write it as a function of the structure of the lens fibers in a particular plane, namely, the equatorial plane. This function would give the appropriate tortuosity for a set of lens fibers packed into a cylindrical array. To pack the fibers into a spheroidal structure, they must taper from equator to pole. The structural parameters that vary from equator to pole are then replaced in the function with their mean values and the mean tortuosity factor is computed. This approach is likely to be reasonably accurate for a quasi-crystalline structure, although a complete analysis should be undertaken once the necessary morphological data are available.

The expression for the tortuosity factor derived by Mathias et al. (1977) is appropriate for the equatorial plane in Fig. 8.

$$\tau = \frac{\frac{N_B}{2}(\delta_N/\delta_B)}{\left(\delta_N \frac{L_T}{A_F}\right)^2}, \qquad \text{(A-2)}$$

where N_B are the number of branches per node in the equatorial plane, L_T/A_F is the length of extracellular space per area of tissue in the equatorial plane, δ_N is the average spacing between nodes in the equatorial plane, δ_B is the spacing between radial branches in the equatorial plane. These parameters are determined from several networks in Mathias et al. (1977, Fig. 11, where the construction of a unit cell and radial dimension Δr is also discussed).

The construction of a unit cell appropriate for the lens is also shown in Fig. 8. The unit cell is a rectangle of smallest dimension which can be replicated to produce the entire network. Thus, it can be used to determine $L_T/A_F = (L_1 + 2L_3)/(2\Delta r)(0.5)(L_1 + L_2)$. The spacing between radial branches equals the mean node spacing, namely, $\delta_N = \delta_B = (0.5)(L_1 + L_2)$. Rae and B. Eisenberg (personal communication) have made preliminary estimates of parameters $L_1 = 8.1\ \mu$m; $L_2 = 9.5\ \mu$m; $L_3 = 1.3\ \mu$m; $2\Delta r = 2.4\ \mu$m, implying $\delta_B = \delta_N = 8.8\ \mu$m and a tortuosity, in the equatorial plane, of 0.08.

The value of tortuosity applicable to the entire preparation can be determined if we assume that

the lens fibers taper in an idealized manner from equator to pole. We assume that the outer surface of each hexagonal unit (the surface generated by L_1) forms a lune of a sphere (Bartsch, 1974, p. 167), with the dimension $L_1(\phi)$ varying from equator to pole, but with the dimension L_3 constant. Because a lune includes the same angle at equator and pole (by definition), it is straightforward to determine the mean value of $L_1(\phi)$ from an integration of $L_1(\phi)$ over ϕ, giving $\bar{L}_1 = (2/\pi)L_1$. Then

$$\tau = \frac{N_B/2}{\left(\frac{\bar{L}_1 + 2L_3}{2\Delta r}\right)^2}. \qquad \text{(A-3)}$$

The resulting mean value of the tortuosity is 0.14.

This work was greatly aided by the technical assistance of Mr. R. McCarthy and the programming of Mr. T. Streicher, who is responsible for the code which processed the data and compared it with theory.

This work was supported in part by National Institutes of Health grants EY 01207 and NS 13778 to J. L. Rae and HL 20230 to R. S. Eisenberg.

Received for publication 16 June 1978 and in revised form 25 September 1978.

REFERENCES

ADRIAN, R. H. 1956. The effect of internal and external potassium concentration on the membrane potential of frog muscle. *J. Physiol. (Lond.).* **133**:631.

BARTSCH, H. J. 1974. Handbook of Mathematical Formulas. Academic Press, Inc., New York. (Translation of the 9th edition of H. Liebscher, *Mathematische Formeln.* Leipzig.) 167.

BENDAT, J. S., and A. G. PIERSOL. 1971. Random Data: Analysis and Measurement Procedures. Wiley-Interscience, John Wiley & Sons, New York. 136–208.

BENEDETTI, E. L., I. DUNIA, C. J. BENTZEL, A. J. M. VERMORKEN, M. KIBBELAAR, and H. BLOEMENDAL. 1976. A portrait of plasma membrane specializations in eye lens epithelium and fibers. *Biochim. Biophys. Acta.* **457**:353.

COHEN, A. I. 1965. The electron microscopy of the normal human lens. *In* Symposium on the Lens. The C. V. Mosby Company, St. Louis, Mo.

CROWE, L. M., and R. J. BASKIN. 1977. Stereological analysis of developing sarcotubular membranes. *J. Ultrastruct. Res.* **58**:10.

DUNCAN, G. 1969. The site of the ion restricting membranes in the toad lens. *Exp. Eye Res.* **8**:406.

DUNCAN, G. 1973. Role of membranes in controlling ion and water movements in the lens. *Ciba Found. Symp.* **19**: 99–116.

EISENBERG, R. S., V. BARCILON, and R. T. MATHIAS. 1979. Electrical properties of spherical syncytia. *Biophys. J.* **25**:151–180.

EISENBERG, R. S., and P. W. GAGE. 1969. Ionic conductances of the surface and transverse tubular membranes of frog sartorius fibers. *J. Gen. Physiol.* **53**:279.

EISENBERG, R. S., and E. A. JOHNSON. 1970. Three dimensional electrical field problems in physiology. *Prog. Biophys. Mol. Biol.* **20**:1.

EISENBERG, R. S., R. T. MATHIAS, and J. L. RAE. 1977. Measurement, modeling and analysis of the linear electrical properties of cells. *Ann. N.Y. Acad. Sci.* **303**:342.

EISENBERG, R. S., and J. L. RAE. 1976. Current-voltage relationships in the crystalline lens. *J. Physiol. (Lond.).* **262**:285.

FISCHMAN, D. A. 1972. Development of striated muscle. *In* The Structure and Function of Muscle. Vol. 1. G. H. Bourne, editor. Academic Press, Inc., New York. 2nd edition. 75–148.

JACK, J. J. B., D. NOBLE, and R. W. TSIEN. 1975. Electric Current Flow in Excitable Cells. Clarendon Press, Oxford. 101–130.

MATHIAS, R. T. 1975. A study of the electrical properties of the transverse tubular system in skeletal muscle. Ph.D. thesis, University of California, Los Angeles.

MATHIAS, R. T., R. S. EISENBERG, and R. VALDIOSERA. 1977. Electrical properties of frog skeletal muscle fibers interpreted with a mesh model of the tubular system. *Biophys. J.* **17**:57.

MATHIAS, R. T., J. L. RAE, and R. S. EISENBERG. 1978. Linear electrical properties of the lens of the eye. *Biophys. J.* **21**:48a. (Abstr.)

OPPENHEIM, A. V., and R. W. SCHAFER. 1975. Digital Signal Processing. Prentice-Hall Inc., Englewood Cliffs, N.J. 532-577.

PATERSEN, C. A. 1970. Extracellular space of the crystalline lens. *J. Physiol. (Lond.).* **218**:797.

PESKOFF, A. 1978. Electric potential in three-dimensional electrically syncytial tissues. *Bull. Math. Biol.* In press.

RAE, J. L. 1973. The potential difference of the frog lens. *Exp. Eye Res.* **15**:485.

RAE, J. L. 1974. The movement of procion dye in the crystalline lens. *Invest. Opthalmol.* **13**:147.

RAE, J. L. 1978. The electrophysiology of the crystalline lens. *In* Current Topics in Eye Research. Vol. 1. J. Zadunaisky and H. Davson, editors. Academic Press, Inc., New York. 37–90.

TOSTESON, D. C. 1964. Regulation of cell volume by sodium and potassium transport. *In The Cellular Functions of Membrane Transport.* J. F. Hoffman, editor. Prentice-Hall Inc., Englewood Cliffs, N.J. 3–22.

TOSTESON, D. C., and J. F. HOFFMAN. 1960. Regulation of cell volume by active cation transport in high and low potassium sheep red cells. *J. Gen. Physiol.* **44**:169.

VALDIOSERA, R., C. CLAUSEN, and R. S. EISENBERG. 1974*a*. Impedance of frog skeletal muscle fibers in various solutions. *J. Gen. Physiol.* **63**:460.

VALDIOSERA, R., C. CLAUSEN, and R. S. EISENBERG. 1974*b*. Circuit models of the passive electrical properties of frog skeletal muscle fibers. *J. Gen. Physiol.* **63**:342.

YORIO, T., and P. J. BENTLEY. 1976. Distribution of the extracellular space of the amphibian lens. *Exp. Eye Res.* **23**:601.